

CEAZ: Accelerating Parallel I/O via Hardware-Algorithm Co-Design of Efficient and Adaptive Lossy Compression

Chengming Zhang
Washington State University
Pullman, WA, USA
chengming.zhang@wsu.edu

Sian Jin
Washington State University
Pullman, WA, USA
sian.jin@wsu.edu

Tong Geng
Pacific Northwest National Laboratory
Richland, WA, USA
tong.geng@pnnl.gov

Jiannan Tian
Washington State University
Pullman, WA, USA
jiannan.tian@wsu.edu

Ang Li
Pacific Northwest National Laboratory
Richland, WA, USA
ang.li@pnnl.gov

Dingwen Tao
Washington State University
Pullman, WA, USA
dingwen.tao@wsu.edu

ABSTRACT

As supercomputers continue to grow to exa-scale, the amount of data that needs to be saved or transmitted is exploding. To this end, many previous works have studied using error-bounded lossy compressors to reduce the data size and improve the I/O performance. However, little work has been done for effectively offloading lossy compression onto FPGA-based SmartNICs to reduce the compression overhead. In this paper, we propose a hardware-algorithm co-design of efficient and adaptive lossy compressor for scientific data on FPGAs (called CEAZ) to accelerate parallel I/O. Our contribution is fourfold: (1) We propose an efficient Huffman coding approach that can adaptively update Huffman codewords online based on codewords generated offline (from a variety of representative scientific datasets). (2) We derive a theoretical analysis to support a precise control of compression ratio under an error-bounded compression mode, enabling accurate offline Huffman codewords generation. This also helps us create a fixed-ratio compression mode for consistent throughput. (3) We develop an efficient compression pipeline by adopting cuSZ’s dual-quantization algorithm to our hardware use case. (4) We evaluate CEAZ on five real-world datasets with both a single FPGA board and 128 nodes from Bridges-2 supercomputer. Experiments show that CEAZ outperforms the second-best FPGA-based lossy compressor by $2\times$ of throughput and $9.6\times$ of compression ratio. It also improves MPI_File_write and MPI_Gather throughputs by up to $25.8\times$ and $24.8\times$, respectively.

1 INTRODUCTION

Today’s high-performance computing (HPC) applications running on leadership supercomputers are essential in many science and engineering domains. Such applications can generate large volumes of scientific data for post-hoc analysis and visualization. However, since the development of storage and networking hardware is much slower than that of computing power and memory capacity [7], the I/O and network bandwidths are becoming the main bottlenecks for HPC applications to achieve high performance at large scales. I/O and communication costs can quickly overwhelm the overall performance as supercomputers grow towards exa-scale. For instance, modern cosmological simulations are widely used by scientists to investigate new fundamental astrophysics ideas, develop and evaluate new cosmological probes, assist large-scale cosmological surveys, and investigate systematic uncertainties [14, 21]. A famous adaptive mesh cosmological simulation code Nyx [1] can generate

up to 2.8 TB of data for a single snapshot under a simulation resolution of 4096^3 , requiring to save a total of 2.8 PB data, when running the simulation for 5 times with 200 snapshots dumped per run.

Such a large amount of data is often generated in parallel manner from a scaled-up number of ranks, on which each holds a proportion of the data and must introduce an extra collective communication to dump the entire snapshot to the file system. This process takes an unprecedented challenge to I/O bandwidths and storage systems on today’s supercomputers [7, 29, 52, 53]. Therefore, it is urgent to develop effective data reduction methods to reduce the sizes of data moved between memories and storage systems. One straightforward approach is decimation, i.e., storing one snapshot every several timesteps during the simulation. However, even with decimation, there are still a number of timesteps to store, and the large amount of data in one timestep can still overwhelm the storage capacity and I/O bandwidth, not to mention this approach may cause a significant loss of valuable information.

A better way to address this challenge is using data compression. The data partition in each rank is compressed before sending it to the storage system via interconnect network. This can reduce both I/O overhead and storage consumption. However, traditional lossless compression can only provide a limited compression ratio to the scientific dataset by usually up to $2\times$ [40]. On the other hand, the new generation of error-bounded lossy compressors such as using SZ [10, 29, 44] and ZFP [30] can provide a much higher compression ratio while only introducing controllable distortion of data. Many prior studies have demonstrated the effectiveness of using those error-bounded lossy compressors for scientific data reduction [7, 10, 18, 24, 25, 29, 30, 33, 34, 44, 45] and improving I/O performance. [16, 37, 54].

While error-bounded lossy compressors on CPUs can provide high compression ratio, their low compression and decompression throughputs unavoidably cause relatively high performance overheads to applications, which often offset the performance benefit gained from saving and loading compressed data with less sizes. Thus, we must develop a high-throughput lossy compressor to effectively accelerate parallel I/O for HPC applications. Recently, both SZ and ZFP teams started to develop and release their GPU and FPGA implementations. On one hand, GPU’s massive SIMT (single instruction, multiple threads) parallelism enables it to achieve high throughput. However, during the lossless compression step of SZ algorithm, encoding and decoding each symbol according to the built Huffman tree [22] with different branches results in random

memory access pattern. This causes serious divergence issues, inevitably leading to low GPU memory bandwidth utilization and performance. On the other hand, field programmable gate array (FPGAs) offer many advantages, such as configurability, high energy efficiency, and low latency[15]. Hence, it is suitable for real-time processing such as streaming big data analytics. Moreover, FPGAs have been a viable and popular option at scale for smart Network Interface Cards (SmartNICs) [12, 38], which are being increasingly used in data centers to offload networking functions from host processors, such as MPI collective operations acceleration [20]. Thereby, this makes FPGA-based SmartNICs ideal platforms for offloading compression to accelerate parallel I/O.

The current state-of-the-art FPGA-based lossy compressor [41] is capable of up to 8 GB/s throughput. However, this 8 GB/s throughput is still much lower than the throughputs of PCIe3, PCIe4, and InfiniBand, which precludes their uses in real application scenarios. But there are several challenges to implement a high-throughput lossy compression on FPGAs: (1) FPGAs usually have much lower clock frequencies (e.g., 800 Mhz at most) compared to CPUs and GPUs. It is difficult to use such low frequency to achieve relatively high throughput. (2) The limited resources on a single FPGA chip prevent us from increasing the throughput by simply adding more compression pipelines. Thus, we must deeply optimize the compression algorithm to effectively utilize the limited hardware resources.

To address these challenges, in this work, we focus on designing an efficient lossy compression algorithm that is suitable for FPGA hardware, and offload it onto FPGA-based SmartNICs to accelerate parallel I/O. Specifically, we propose a hardware-algorithm co-designed efficient and adaptive lossy compressor (zip) (CEAZ), which is capable of providing both high compression ratio and high throughput. CEAZ adopts a dual quantization strategy [48] to completely remove data dependency and instantiates multiple pipelines to process input data in parallel. Unlike cuSZ that implements dual-quantization using massive GPU threads, we implement the dual quantization in CEAZ using a pipelined manner, which is more suitable for FPGA architecture. Moreover, different from existing FPGA-based lossy compressors such as GhostSZ [56] and waveSZ [47] that statically build trees in Huffman coding for every data chunk, CEAZ dynamically determines whether to update codewords by building a new tree or use previous/offline codewords according to the distribution of current symbol frequencies, leading to a high throughput. As a result, CEAZ can efficiently and effectively reduce the data size and significantly increase the parallel I/O performance, which can benefit any HPC applications that face the challenge of saving and loading large amounts of data in parallel. The contributions of this work are summarized as follows:

- We propose an efficient Huffman coding approach that can adaptively update Huffman codewords online for any given dataset based on our offline Huffman codewords, which are generated from a variety of representative scientific datasets. It can reduce the data dependency in Huffman coding and dramatically improve the compression throughput.
- We derive a theoretical analysis to support a precise control of compression ratio under the error-bounded compression mode, which can align quantization-code histograms of different datasets and enable an accurate generation of offline Huffman

codewords. It also helps us develop a fixed-ratio compression mode for consistent throughput, which is important to guarantee a consistent throughput in data transfer.

- We develop an efficient compression pipeline by adapting the dual-quantization algorithm to our hardware use case.
- We evaluate CEAZ with five real-world scientific datasets in both serial and parallel. Experiments demonstrate that CEAZ outperforms the state-of-the-art solution by 2× of throughput and 9.6× of compression ratio on a single FPGA board. Moreover, CEAZ can improve the throughputs of MPI_File_write and MPI_Gather by up to 25.8× and 24.8×, respectively, with 128 nodes from Bridges-2 supercomputer.

The rest of this paper is organized as follows. In Section 2, we discuss the background and our research challenges. In Section 3, we present the design of our proposed FPGA-based error-bounded lossy compressor CEAZ. In Section 4, we evaluate CEAZ on various scientific datasets and present the results on compression quality, compression throughput, and parallel performance. In Section 5, we summarize our conclusions and provide ideas for future works.

2 BACKGROUND AND MOTIVATION

In this section, we first present background information about scientific data compression and FPGA-based lossy compression. We then discuss the challenges and our research motivations.

2.1 Floating-Point Data Compression

Floating-point data compression has been studied for decades. The data compressors can be split into two categories: lossless compression and lossy compression. In comparison to lossy compression, lossless compression such as FPZIP [31] and FPC [6] can only provide limited compression ratios (typically up to 2:1 for most scientific data) due to the significant randomness of the ending mantissa bits, especially for large scientific floating-point data [40].

Lossy compression, on the other hand, can compress data with little information loss in the reconstructed data. Compared to lossless compression, lossy compression can provide a much higher compression ratio while still maintaining useful information for scientific discoveries. Many lossy compressors supporting floating-point data were proposed and designed for visualization. Thus, many lossy compressors employ the techniques directly inherited from lossy compression of images, such as variations of wavelet transforms, coefficient prioritization, and vector quantization. Lossy compressors for image processing are designed and optimized considering human perception, such as JPEG2000 [46]. While such compressors may be adequate for visualization purposes, they do not provide error controls on demand for scientific studies. For example, most lossy compressors designed for visualization do not provide control of a global upper bound on the compression error (the maximum compression error).

In recent years, a new generation of lossy compressors for scientific floating-point data has been proposed and developed, such as SZ [10, 29, 44, 48] and ZFP [9, 30]. Both lossy compressors can provide multiple compression modes, such as error-bounded mode and fixed-rate mode to introduce error control or compression ratio control. Error-bounded mode requires users to set an error bound, such as absolute error bound or point-wise relative error bound.

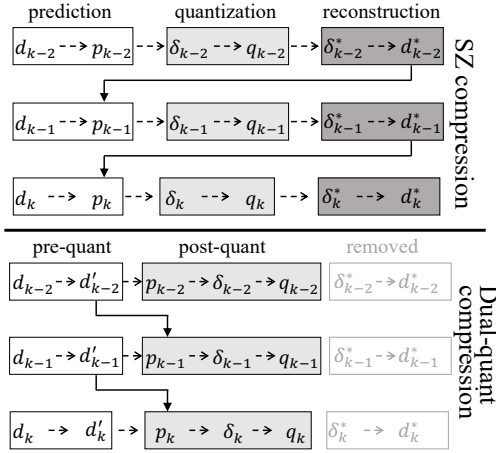


Figure 1: Diagram of original SZ (top) and dual-quantization-based compression (bottom). Arrows indicate data dependency.

The compressor ensures the differences between the original data and the reconstructed data do not exceed the user-set error-bound. Fixed-rate mode means that users can set a target bitrate, which is the average bits used to encode each data point, and the compressor guarantees that the actual bitrate of the compressed data to be lower than the user-set value.

Compared to ZFP which utilizes Discrete Fourier transform to manipulate data information, SZ predicts each data point’s value by its neighboring data points in a multidimensional space with an adaptive predictor (mainly using a Lorenzo predictor [23]). Next, it performs an error-controlled linear-scaling quantization to convert all floating-point values to an array of integer numbers. Lastly, it performs a customized Huffman coding and lossless compression to shrink the data size significantly. This helps SZ provide a unified error distribution between original and reconstructed data within the user-set error-bound range, which fully utilizes the error tolerance space and provides a high compression ratio [10, 29, 33, 43, 44].

SZ was first developed for CPU architectures, and has released the CUDA implementation (called cuSZ) [48]. cuSZ proposed a dual-quantization approach that first quantizes the dataset to eliminate the data dependency and then enables a fully parallel prediction. Specifically, as shown in Figure 1, in the original SZ algorithm, the current compressed data point q_{k-2} must be reconstructed before compressing the next point d_{k-1} , causing the data dependency issue. The dual-quantization scheme can remove the reconstruction step so that we can compress all data points independently. We refer readers to [48] for more details about dual-quantization scheme.

Compared to lossy compression on CPUs, GPU-based lossy compression can provide much higher throughput for both compression and decompression [24]. cuSZ [48] and cuZFP [9] are existing GPU-accelerated implementations of SZ and ZFP, respectively, which create massive GPU threads to parallelize the computation. GPU implementations are capable of achieving dozens of GB/s throughput of compression and decompression. However, These same approach are not very efficient on FPGAs, which have much lower clock frequencies compared to GPUs. And the FPGA chip space limitations prevent fitting too many instances of compression/decompression

pipelines on chip. But, FPGA implementations offer several advantages over GPU implementations. (1) FPGAs can inherently provide low latency as well as deterministic latency for real-time applications. (2) FPGAs provide a high degree of user customization, and their implementations are easier to be integrated into other systems. (3) FPGAs provide relatively lower power consumption (e.g., 40 watts) than a single GPU (e.g., over 200 watts).

2.2 FPGA-based Lossy Compression

Existing works have shown that significant performance speedups can be achieved by offloading lossy compression onto hardware. GhostSZ [56] is the first implementation of SZ-1.0 [11] lossy compression on FPGAs. GhostSZ improves throughput by $10 \times -85 \times$ over the SZ and provides 25% higher compression ratio with a similar peak signal-to-noise ratio (PSNR). However, SZ-1.0 is a deprecated version which suffers from low prediction accuracy thus results in low compression ratios. The prediction method used by GhostSZ may cause a significant waste of FPGA computation resources and a workload imbalance issue, as demonstrated in [47].

waveSZ [47] is another hardware implementation of SZ lossy compression. It adopts a wavefront memory layout to fit into SZ algorithm to alleviate the data dependency during the prediction process. It improves the compression ratio and throughput by $2.1 \times$ and $5.8 \times$, respectively, over GhostSZ. However, waveSZ has several drawbacks in terms of both compression ratio and throughput: (1) waveSZ just alleviates the data dependency using wavefront memory but does not eliminate it. As a result, its throughput does not exceed 1 GB/s. (2) The wavefront memory layout involves rearranging data before compression, and this overhead would be relatively high when processing a large amount of data. (3) waveSZ only focuses on accelerating the prediction stage without handling the high overhead of Huffman coding. However, Huffman coding is the main bottleneck after fully removing the data dependency in prediction (will be discussed in Section 2.4).

BurstZ [41] is a variant of the 1-dimensional ZFP algorithm and also implemented onto FPGAs. BurstZ can provide a high-throughput (8 GB/s), but it suffers from a significantly lower compression ratio drop compared with the original ZFP algorithm. For example, the original ZFP algorithm achieves $21 \times$ compression ratio on the NWChem dataset [36] with an error bound of 0.001, whereas BurstZ only achieves $4.7 \times$ compression using the same error bound. Besides, the 8GB throughput is much smaller than the throughput of current PCIe3, PCIe4, and InfiniBand. In addition, ZHW [57] is an FPGA-based lossy compressor based on the ZFP algorithm. But different from ZFP, ZHW is not error-bounded, so we take BurstZ as the current state-of-the-art FPGA implementation of ZFP and compare CEAZ with it in our evaluation.

2.3 MPI Collectives and MPI-I/O

Message Passing Interface (MPI) [17] contains two main types of operations related to parallel I/O, i.e., collective operations and MPI-IO operations. MPI collective operations include scatter, gather, prefix scan, reduce, etc. Collective operations play an important role in many HPC applications, which often rely on collective communication among multiple processes. The key concept in MPI is the communicator. A communicator defines a group of processes that

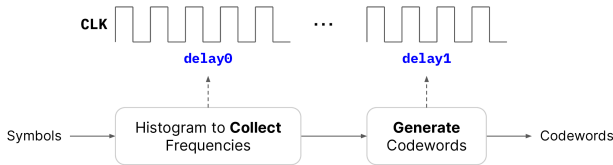


Figure 2: Two necessary delays in codewords generation.

have the ability to communicate with one another. In this group of processes, each is assigned a unique rank, and they explicitly communicate with one another by their ranks. The foundation of communication is built upon send and receive operations among processes. In this paper, we focus on gather (MPI_Gather) operation, which is a representative MPI collective operation and used by many parallel I/Os. In detail, MPI_Gather takes elements from many processes and gathers them into one single process.

MPI-IO is a fundamental HPC middleware for parallel I/O. Many parallel I/O systems such as parallel HDF5 [13] and ADIOS [32] are built based on it. In MPI-IO, data is moved between files and processes by issuing read and write calls. The data access routines can be individual or collective. By using a collective routine, processes are coordinated with each other to optimize access to I/O device.

2.4 Research Challenges

High Overhead of Huffman Coding. Given a set of symbols, Huffman coding generates codewords based on the evidence that not all symbols have the same probability. Instead of using fixed-length codewords, Huffman compression uses variable-length codewords based on the relative frequency of different symbols. A fixed-length code assumes equal probability for all symbols and hence assigns the same length codewords to all symbols. In contrast to fixed length codes, Huffman compression is based on the principle to use fewer bits to represent frequent symbols and more bits to represent infrequent symbols. Even though variable-length codewords can provide high compression ratio in our scenario, Huffman compression has high overhead in terms of latency, area, and power [28]. Moreover, to achieve high compression and throughput, certain key challenges should be addressed.

Challenge of Codewords Generation. The first challenge is to build a Huffman tree and generate codewords within limited hardware clock cycles to meet high-throughput requirements. Our goal is to accelerate MPI collective I/O in real time through compression. So we hope to reduce the compression latency as much as possible. Figure 2 shows two necessary delays when generating codewords. We need to collect enough symbols delay0 so that the distribution of symbol frequencies is representative. delay1 is around 19,000 cycles in the worst case as shown in Figure 6. In addition, generating codewords needs 7 steps: filter, sort, create tree, compute

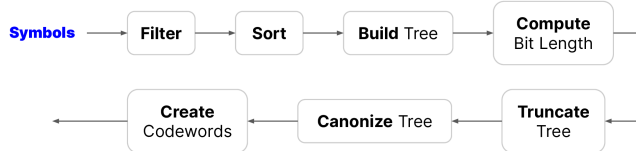


Figure 3: The process of canonical Huffman encoding.

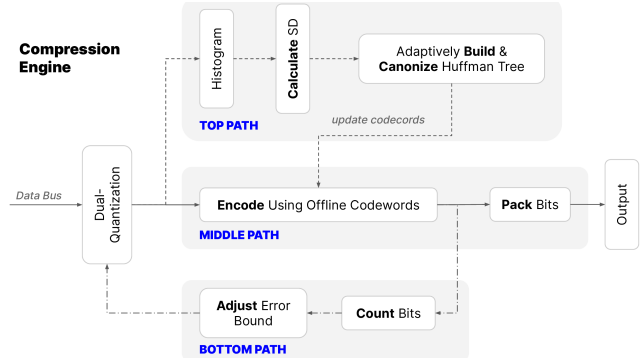


Figure 4: Design of our proposed lossy compression engine CEAZ.

bit length, truncate tree, canonize tree and create codewords, as illustrated in Figure 3. This procedural is a serial process that is hard to be parallelized by FPGAs or GPUs. We make full use of the characteristics of the FPGAs to speed up this process by pipeline. But the latency presented in Figure 6 is still relatively large.

Challenge of Predefined Codewords. Inspired by E^2MC [28], we will use predefined codewords at the beginning and update the codewords during the running time. This method introduces the second challenge: how can we generate suitable codewords which can cover the features of all the scientific datasets?

3 DESIGN METHODOLOGY

In this section, we describe the design of our proposed FPGA-based lossy compressor CEAZ and parallel I/O accelerator.

3.1 Overview of CEAZ Compression Engine

We show our proposed lossy compression engine in Figure 4. It has three main dataflow paths. On the top dataflow path, we preprocess float-point data using dual quantization algorithm [48] (abbreviated as dual-quant), which generates integers as symbols for the following Huffman coding. We collect frequencies of symbols using histogram and calculate the standard deviation (SD) of frequencies. According to the SD value, we will decide whether to build a new Huffman tree based on the symbol frequencies or not (will be discussed in the next section).

Figure 5 shows our dual-quant pipeline design. Dual-quant is a novel two-phase prediction-quantization approach, which can completely eliminate the data dependency in the prediction and quantization steps. Our dual-quant consists of two steps: prequantization and postquantization. Given a float point data d , we first quantize it based on the user-set error bound and convert it to an integer data d' . After the prequantization, we can calculate its predicted value based on its neighboring values (denoted neighboring(d')) using

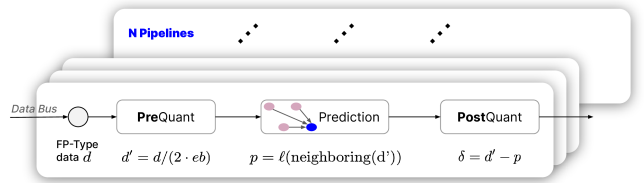


Figure 5: Design of our adopted dual-quantization pipeline.

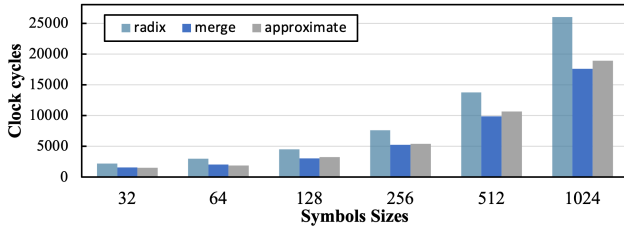


Figure 6: Latency of our Huffman coder with different symbol sizes.

Lorenzo predictor (denoted ℓ), $p = \ell$ (neighboring(d')). The second step, called postquantization, computes the difference δ between the predicted value and the pre-quantized value. δ will be compressed by Huffman compression. Since the dual-quant part has no data dependency, we could instantiate N pipelines to process N float-point data in parallel. On the middle dataflow path, we directly encode symbols using existing codewords for seeking high throughput. The encoder can find the codeword corresponding to each symbol and output it. We then pack variable-length encoded (compressed) symbols to save the storage space. On the bottom dataflow path, we feed back total bits of encoded symbols to estimate compression ratio, and then adjust the error bound.

Our proposed compression engine has two working modes: fixed accuracy (i.e., error bounded) and fixed ratio (i.e., fixed bit-rate). The fixed-accuracy mode ensures information loss of compressed data is within the specific error bound, whereas the fixed-ratio mode ensures the transfer of compressed data has a consistent throughput. For the fixed-accuracy mode, we need to define an upper bound of errors that can be tolerated by applications and keep using this error bound through the whole compression process. For the fixed-ratio mode, we can set a suitable error bound to achieve a target compression ratio, as a higher error bound leads to a higher compression ratio. Specifically, we use the following steps to adjust the error bound: (1) We estimate the compression ratio by $C = \frac{\text{TotalBits}(\text{original data})}{\text{TotalBits}(\text{compressed data})}$, where $\text{TotalBits}(\text{original data}) = W * N$. Here W is the bit-rate of original data. For single/double floating-point data, W is 32/64 bits per value. N is the total number of data points that have been compressed. (2) We calculate the compressed bit-rate and target bit-rate as follows: $B = \frac{W}{C}$ and $B_{\text{target}} = \frac{W}{C_{\text{target}}}$. (3) We adjust the error bound by Equation 2.

3.2 Efficient and Adaptive Huffman Coder

3.2.1 Fast approximate sort based on Lorenzo predictor's feature.

In order to build the Huffman tree, we must sort the symbols based on their frequencies after we filter out symbols with a frequency of zero. A few previous works [26, 50] use radix sort to reduce the utilization of hardware resources. However, we find that radix sort typically takes more than 30% of the total time when we break down the execution time of generating codewords. This is because the time complexity of radix sort is $O(d \times (n + b))$ (where b is the base for representing numbers and d is the number of digits of the maximum possible value) with $d = 32$ and $b = 10$ typically.

Inspired by [26], we replace radix sort with merge sort. This is because merge sort has a lower time complexity (i.e., $O(n \log n)$) than radix sort (i.e., $O(d \times (n + b))$) considering $\log n$ is relatively small such as 10 (lower than $d = 32$) in our case. We adopt the non-recursive way of merge sort in our hardware implementation.

Algorithm 1: Proposed fast sort based on Lorenzo predictor's feature.

Result: A approximately sorted array

```

1 S: defined structure contains two members: symbol, and its frequency
2 A: input array, its data type is S, len: length of input array, i: index of A
3 p: index of symbol 513 in A, m: index of the midpoint of A, l: index, h: index
4 O: output sorted array, j: index of O
5 t: loop count
6 l = p - 1, h = p + 1, j = len - 2
7 O[len - 1] = A[p]
8 if p ≤ m then
9   | t = p
10 else
11   | t = len - p - 1
12 end
13 for i ← 1, t do
14   if A[l].frequency ≤ A[h].frequency then
15     | O[j] = A[h]
16     | O[j - 1] = A[l]
17   else
18     | O[j] = A[l]
19     | O[j - 1] = A[h]
20   end
21   l = l - 1, h = h + 1, j = j - 2
22 end
23 /* copy remaining data from A to O */
24 CopyRemaining(A, O)

```

However, we identify that Vitis HLS we use requires the size of the array to be sorted is a constant and a power of two, which prevents us from using the original merge-sort hardware implementation. This is because the non-zero frequencies to be sorted in our case are neither fixed nor the power of two. Furthermore, we note that the frequencies of symbols that are generated by Lorenzo predictor and linear-scaling quantization [44] are symmetric, as shown in prior studies [25]. We verify this in our experiments with 1024 symbols, as shown in Figure 7 (symmetric with respect to symbol 513). This feature inspires us to use an approximate sort to improve the efficiency, since Huffman coding can accept the approximately sorted symbols, which would not notably degrade the compression ratio. Specifically, assuming A is an unsorted array with symbols, and O stores sorted symbols. We have two indices, l and h . l is initialized to the index of the symbol to the left of the middle symbol (e.g., 512), and h is initialized to the index of the symbol to the right of the middle symbol. We compare the frequencies of symbols with indices l and h , get the correct order of these two symbols, and store them in the corresponding positions in O . Then, we decrease l by 1 and increase h by 1. We will repeat the above process until the entire symbols are sorted.

We describe our proposed approximate sort algorithm in Algorithm 1 in detail. It has the time complexity of $O(\frac{n}{2})$, which is lower than the time complexity of radix sort and merge sort. We compare the total time of Huffman coding with different sort algorithms using 1024 symbols. The results shown in Figure 6 illustrate that our approximate sort saves the total Huffman coding time by up to 27% over the second-best radix sort. More details about our experimental platform will be presented in Section 4.

3.2.2 Offline Huffman codewords generation.

On the premise of meeting the acceptable reduction in compression ratio, we propose to combine offline and online Huffman codewords generation strategies in order to improve the throughput as much as possible. As shown in figure 4, the symbols generated at the beginning by dual-quant will be encoded by offline codewords directly; at

the same time, we also collect the frequencies of symbols. We will generate new Huffman codewords if the change of standard deviation of symbol frequencies is greater than the threshold τ . τ is a hyper-parameter, and we will discuss it in the next section.

We generate offline codewords based on the following three steps: (1) We set a suitable error bound to let our compressor have a similar compression ratio on different datasets. (2) We collect symbol frequencies on different datasets. (3) We calculate the average symbol frequencies from collected frequencies. The average symbol frequencies are used to generate offline codewords. In order to make offline codewords representative and promising for high compression ratio, we collect symbol frequencies based on all the real-world datasets from the Scientific Data Reduction Benchmarks (SDRBench) [39]. Figure 10 shows the compression ratio degradation by using the offline codewords, which is acceptable.

Using different error bounds to compress the same dataset results in different histograms of quantization codes (i.e., different distributions of symbol frequencies). For example, using a larger error bound results in a tighter histogram of quantization codes compared to using a smaller error bound. In extreme cases where very large error bounds are used, there can be only a few quantization codes for Huffman coding. In order to make the offline codewords adaptive for a wide range of datasets, we must choose suitable error bounds for multiple scientific datasets, which can result in a similar histogram of quantization codes after Lorenzo predictor. In another word, we must control the error bound for each dataset to provide a similar compression ratio. Instead of using a trial-and-error approach to search the suitable error bound for every dataset, we provide a theoretical analysis to predict the error bound given a target ratio based on one-time sampling.

A naive solution to align different datasets with a similar compression ratio is to use the same value-ranged-based relative error bound instead of the same absolute error bound. Which eventually provides an absolute error bound based on the value range of the given dataset. While using the same value-ranged-based relative error bound for different datasets can reduce the range divergence of their quantization-code histogram, it cannot guarantee the compression ratio of different datasets is similar to each other. In our experiment, we identify the compression ratio range of 4~13 \times when using the same value-ranged-based relative error bound for multiple scientific datasets. Our proposed solution considers the efficiency of Huffman coding affected by error bound to accurately estimate the error bound for a target compression ratio. We assume the bit-rate (i.e., average bit length of each data point) of quantization code after Huffman encoding is:

$$\text{mean}(L) = \sum_{i=0}^n P(s_i)L(s_i) \approx \sum_{i=0}^n P(s_i) \log_2 P(s_i), \quad (1)$$

where n is the number of different Huffman code, P is the probability of given code s_i , L is the length of given code s_i . We further represent the Huffman code length based on its probability with binary base-2 numeral system. Note that in our case, 1024 symbols are used for Huffman coding and thus are sufficient for this simplification. Consider a given error bound eb can provide a bit-rate of B , when double the error bound to $2eb$, the quantization-code histogram also shrinks accordingly where the total number of symbols is reduced

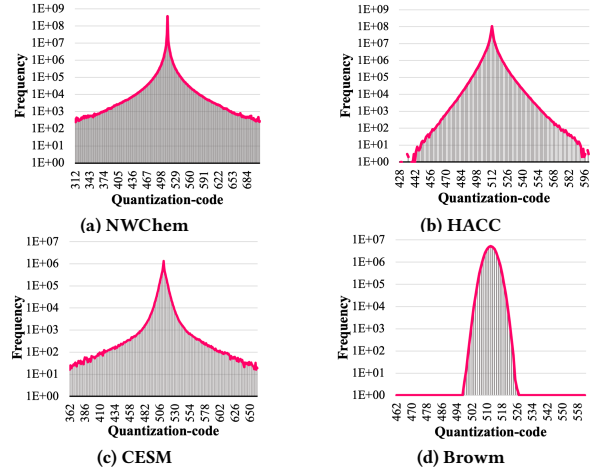


Figure 7: Distribution of symbol frequencies on four scientific datasets, i.e., NWChem [36], HACC [19], CESH [8], and Brown [5]. by 2 \times and the possibility of each symbol is increased by 2 \times . In which case the bit-rate should be:

$$\begin{aligned} B' &= \sum_{i=0}^{n/2} P'(s_i) \log_2 P'(s_i) \approx \sum_{i=0}^{n/2} 2P(s_{2i}) \log_2 2P(s_{2i}) \\ &\approx \sum_{i=0}^{n/2} (P(s_{2i-1}) \log_2 P'(s_{2i-1}) + P(s_{2i}) \log_2 P'(s_{2i})) - 1 \\ &= B - 1 \end{aligned} \quad (2)$$

Thus, we conclude that by doubling the error bound, the bit-rate should add 1. This is also consistent continuous error bound: if compression bit-rate is B under error bound eb , then under new error bound $2eb$ the predicted bit-rate is $B' = B - \log_2 N$. Note that the SZ algorithm uses previous data points' quantized values to predict the value of current point based on Lorenzo prediction, which means different error bounds would affect the shape of quantization-code histogram. However, based on our experiments, this only applies to very large error bounds and hence few quantization bins. In our case, we simplify this to a fixed quantization-code histogram shape under different error bounds, thus a precise 2 \times shrink when doubling the error bound.

With the above analysis, we can simply compress each scientific dataset once with the same value-ranged-based relative error bound eb and compute the optimized error bound eb' for the target bit-rate B_{target} based on the current bit-rate B by $eb' = 2^{B-B_{\text{target}}}eb$.

3.2.3 Adaptive online codewords update. In general, on one hand, the more frequently we update the codewords, the closer we can get to the optimal codewords in terms of compression ratio. On the other hand, too frequently updating codewords may decrease the compression ratio, since the newly generated codewords need to be stored. Moreover, if we do not update the codewords, the compression ratio may decrease as well, because the old codewords are too outdated to reflect current distribution of symbol frequencies. In order to solve this problem, we use two effective metrics to determine when to generate new codewords: (1) storage overhead of codewords and (2) change of distribution of symbol frequencies.

Suppose we have S symbols and S codewords. Each codeword is B bits after canonization process. We have $\text{size}(\text{codewords}) = S \times B$.

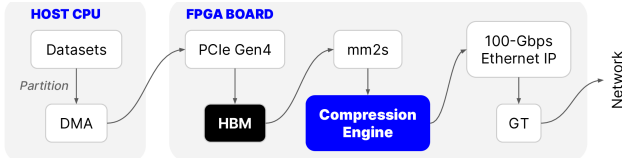


Figure 8: Overview of system architecture integrated with CEAZ.

Our target compression ratio is C . The bit-rate of original data is W . For single/double floating-point data set, the bit width is 32/64 bits per value. The bit rate R is $\frac{W}{C}$. Bit rate R can also be regarded as an average bit length of compressed data. We have $size(compressed\ data) = R * N$, where N is the total number of original data. Assume the codewords is O percentage of compressed data. $O = \frac{size(codewords)}{size(compressed\ data)}$. We set the storage overhead of codewords to be 10%. We have $\frac{S \times B}{S \times B + C \times N} \leq 10\%$. For example, we have 1k ($k=1024$) symbols, and each codeword consumes 8 bits. If we set the target compression ratio to be 10, then we have $N > 24k$.

The symbols generated by dual-quant present a centralized and symmetric distribution, as shown in Figure 7. The generated codewords are highly related to the distribution of symbol frequencies [2]. These good characteristics inspire us to evaluate the similarity of two sets of symbol frequencies using standard deviation. Specifically, assume σ_0 is the standard deviation obtained from the previous data chunk, and σ_1 is the standard deviation obtained from the current data chunk. The change of standard deviation is $\chi = |\sigma_0 - \sigma_1|$. We define a set of thresholds τ_x and propose the following strategy:

- We will not generate new codewords if $\chi \leq \tau_0$ (two similar distributions of symbol frequencies generate almost identical codewords) but keep using the old codewords;
- We will generate new codewords if $\tau_0 < \chi \leq \tau_1$;
- We will use the offline Huffman codewords if $\chi \geq \tau_1$.

We are processing data that is completely different from the previous data if distribution changes drastically. We need to clear histogram of compression engine and collect new symbol frequencies. We set τ_0 and τ_1 as 5.18 and 9.69, respectively, after comprehensive experiments (will be discussed in detail in Section 4.6).

Note that our design is different from other Huffman coding works in terms of adaptivity. For example, Tian et al. [49] proposed a reduction-based scheme for GPUs that iteratively merges the encoded symbols and adaptively determines the number of merge iterations. However, CEAZ only builds a new codebook for the data chunk when the change of its histogram exceeds a threshold in order to target FPGA with limited resources and low clock frequency.

3.3 Parallel I/O Accelerator

Figure 8 shows the overview of our system architecture integrated with CEAZ compression engine. Our system includes two parts: (1) The host is to partition the input dataset and feed the chunked data through the PCIe. Raw data is buffered in high-bandwidth memory (HBM) with 460 GB/s bandwidth and converted into stream data by memory to stream (mm2s) unit. (2) Compression engine compresses the stream data in real-time and outputs compressed data. Ethernet intellectual property (IP) packs the compressed data according to the network protocol. QSFP28 (fiber optical transceiver) gigabit transceiver (GT) finally outputs packed data into network.

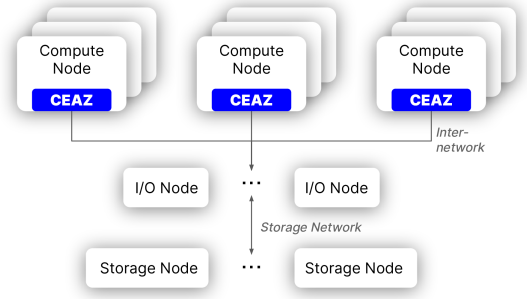


Figure 9: Overview of CEAZ-supported parallel I/O system.

Many scientific applications such as cosmology simulations need to periodically dump a huge amount of raw simulation data to the storage for post-hoc analysis and visualization after simulations. Data across all computing nodes need to be aggregated to the storage node(s). Even though state-of-the-art supercomputers are using InfiniBand interconnect (e.g., 200 Gb/s), it can take up to hours to complete the data aggregation and save (e.g., 1.5 TB/s of aggregated I/O bandwidth and 4.85 PB memory capacity in Fugaku supercomputer [35]). Therefore, we propose to apply CEAZ to the future HPC systems, as shown in Figure 9.

Specifically, CEAZ is directly integrated into the FPGA-based SmartNIC¹ in each computing node and used to compress the raw data before transmitting it to the storage system via interconnection network. There are two main scenarios to use the CEAZ-compressed data in the storage: (1) Checkpoint/restart: to restart the application, the system needs to load the compressed checkpoint from the storage back to each computing node through the FPGA-based SmartNIC, and the decompression engine of CEAZ will reconstruct the whole dataset/checkpoint and pass it to the CPU memories for the application. (2) Post analysis and visualization: users can use the CPU version of our lossy compressor to only decompress the data needed for analysis and visualization, instead of loading the whole compressed data back and relying on the decompression engine in CEAZ. Therefore, there is no need to change the storage system to adapt to our design, since the data is compressed (decompressed) before (after) sending (receiving) to (from) the network adapter.

Note that in the following evaluation, we use Xilinx Alveo U280, which has the same type of FPGA chips (i.e., Virtex Ultrascale+) as Xilinx Alveo SN1000 (SN1000 is the industry’s first SmartNIC offering software-defined hardware acceleration for all function offloads in a single platform). Our evaluation shows that CEAZ only consumes 26K LUT and can be well fitted into mainstream SmartNICs (will be presented in Table 2). Due to significantly reducing the data size (thanks to our effective compression algorithm) and successfully offloading the compute-intensive compression task, CEAZ can accelerate the parallel I/O operations in HPC systems.

¹FPGA-based SmartNIC is a network interface card (network adapter) that offloads processing tasks that the system CPU would normally handle. Using its own on-board FPGAs, the FPGA-based SmartNIC can perform any combination of encryption/decryption, firewall, TCP/IP and HTTP processing, and other networking tasks.

4 EXPERIMENTAL EVALUATION

In this section, we evaluate our proposed FPGA-based error-bounded lossy compressor CEAZ and demonstrate its effectiveness in two perspectives: (1) the effectiveness of the proposed adaptive compression algorithm and the performance (i.e., latency and throughput) of its accelerator implementation, and (2) the improvement of parallel I/O supported by CEAZ with different scales.

4.1 Experimental Setup

4.1.1 Experimental Platform. We use two platforms as our testbed. The first platform is Xilinx Alveo U280 Data Center accelerator card, which is equipped with a PCIe Gen4x8 with CCIX to leverage the latest server interconnect infrastructure for high-bandwidth host processors, 8GB HBM2 and 32GB on-board DDR4 DRAM. CEAZ is implemented with Xilinx Vitis unified software platform (v.2020.1) [51]. The second platform is Bridges-2 [3], which is the newest supercomputer at Pittsburgh Supercomputing Center (PSC). Bridges-2 has 504 nodes (each has two 64-core AMD EPYC 7742 CPUs and 256+ GB RAM), Mellanox ConnectX-6 HDR InfinBband 200Gb/s Adapter, and 15 PB Lustre parallel file system (with 142 GB/s storage bandwidth) [4]. Bridges-2 also has 24 GPU nodes, and each is equipped with eight NVIDIA SXM2 32 GB V100 GPUs. We perform our GPU experiments on one GPU node.

4.1.2 Test Datasets. In order to conduct our evaluation and comparison under realistic scenarios, we use six real-world datasets from the Scientific Data Reduction Benchmarks (SDRBench) [39]: ① 1D HACC cosmology particle simulation [19]. ② 1D NWChem two-electron repulsion integrals computed over Gaussian-type orbital basis sets [36], ③ 1D Brown Samples synthetic and generated to specified regularity [5], ④ 2D CESM-ATM climate simulation [8], ⑤ 3D S3D Combustion simulation [27]. ⑥ 3D NYX AMR-based cosmology simulation [19]. More details can be found in Table 1.

Table 1: Test datasets from Scientific Data Reduction Benchmarks.

	# fields	type	dimensions	size
HACC	6	float	280,953,867	6.3 GB
NWChem	3	double	539,016,059	12.1 GB
Brown	3	double	33,554,433	768.0 MB
CESM	77	float	1,800×3,600	1.9 GB
S3D	11	double	500×500×500	10.2 GB
NYX	6	float	512×512×512	3.0 GB

4.2 Resource Utilization and Clock Frequency

Table 2 shows the breakdown of hardware resource utilization of CEAZ. We implement 16 pipelines for single-precision datasets and 8 pipelines for double-precision datasets. The BRAM_18K is dual-port RAM module instantiated into the FPGA for on-chip storage, and its size is 18k bits. DSP block is an arithmetic logic unit. FF represents for flip-flop. LUT is the basic building block of an FPGA and is capable of implementing any logic function. Note that our LUT consumption is very close to BurstZ’s (only 1.6% higher). The running frequency based on our measurement is slightly lower than the clock frequency we set (i.e., 265 MHz) but is still around 260 MHz. Note that N/A means the utilization data is not provided in the BurstZ work [41].

Table 2: Hardware resource utilization.

	board	BRAM_18K	DSP	FF	LUT	percent
BurstZ	VCU118	N/A	N/A	N/A	25600	<5%
CEAZ	U250	165	0	17285	26008	<1%

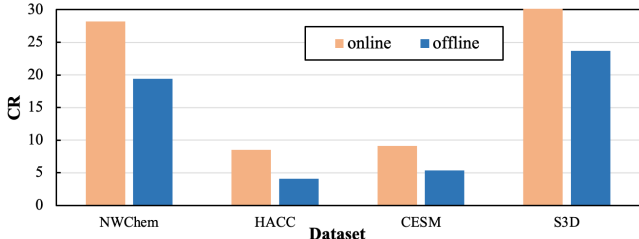


Figure 10: Comparison of compression ratio (CR) between offline codewords and online codewords.

4.3 Power Consumption Discussion

Table 3 shows the comparison of power consumption of hardware used in different implementations. We use Xilinx Power Estimator (XPE) [55] to estimate the power consumption of the Vertex FPGA chip in U280. We use NVIDIA System Management Interface [42] (i.e., nvidia-smi) to get the runtime power consumption of the V100 GPU. We get the power consumption of the whole FPGA and GPU boards from their user guide. As a result, we estimate that CEAZ can save up to 16.3× power consumption, compared to the GPU implementation cuSZ. Note that our CEAZ only dominates up to 1% resources, as shown in Table 2.

Table 3: Power consumption of different hardware.

chip	FPGA		GPU	
	board	chip	chip	card
4w	30w	65w	300w	

4.4 Evaluation on Offline Codewords

We use predefined (offline) codewords at the beginning of the compression process. To prove the effectiveness of our predefined codewords, we evaluate four datasets (i.e., NWChem, HACC, CESM, and S3D) using these codewords with the same value-ranged-based relative error bound of 1e-4 and compare their compression ratios with the optimal ones, as shown in Figure 10. The orange bars represent the ideal compression ratio achieved by first building Huffman tree and then generating accurate codewords. The blue bars represent the compression ratio by directly using our offline codewords. The compression ratio drops on NWChem, CESM, S3D are 23.3% ~ 51.7%. The compression ratio degradation on HACC is more obvious (i.e., about 51.7%), this is because Lorenzo predictor has low efficiency on HACC dataset, and the distribution of quant code generated by Lorenzo predictor has no good statistical effect. We note that even though HACC’s compression ratio drops more than 51.7%, the compression ratio over 4× can still relieve the communication pressure to a certain extent thanks to our high throughput (will be discussed in Section 4.9).

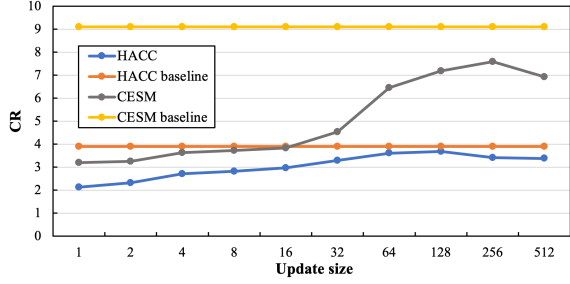


Figure 11: Compression ratios with different update sizes.

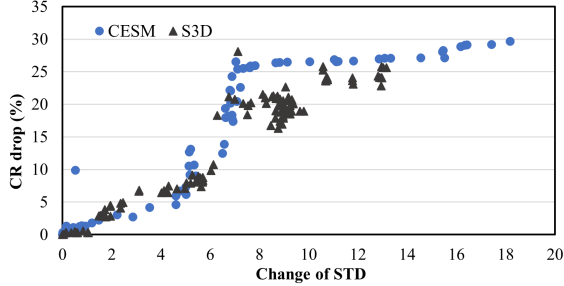


Figure 12: Compression ratio drops with different changes of STD.

4.5 Evaluation on Codewords Update Frequency

As aforementioned, frequently updating codewords will decrease the compression ratio due to the overhead of saving codewords. We evaluate the impact of update frequency on the final compression ratio. We perform the experiments on both CESM and HACC datasets. We set the error bound to the value-range-based relative error bound of 0.0001. We choose to update the codewords every 1 MB, 2 MB, 4 MB, 16 MB, 32 MB, 64 MB, 128 MB, 256 MB, and 512 MB. Figure 11 shows a trend that the compression ratio is significantly reduced when the update size is smaller than 32, because the overhead of storing the codewords is relatively large. Moreover, we also observe that the compression ratio decreases when the update size is larger than 256 MB. The reason is that the codewords are outdated to reflect the current symbols frequencies. These observations are highly consistent with our theoretical analysis. Therefore, we choose 32 MB as our default update size.

4.6 Evaluation on Change of Standard Deviation of Symbol Frequencies

As aforementioned, we use the change of standard deviation of symbol frequencies (i.e., $\chi = |\sigma_0 - \sigma_1|$) to determine when to generate new codewords, use old codewords, or use offline codewords. Using previous codewords under a large χ (a large difference between current and previous distribution) results in a notable drop of compression ratio, while generating new codewords under a small χ (a small difference between current and previous distribution) leads to a high overhead of Huffman coding. Thus, we use experiments to find the suitable thresholds τ_0 and τ_1 . As shown in Figure 12, the drop of compression ratio is less than 5% when $\chi \leq 9.69$, while the drop is over 25% when $\chi \geq 5.18$. So, we set τ_0/τ_1 to 5.18/9.69 to meet both requirements on compression ratio and performance.

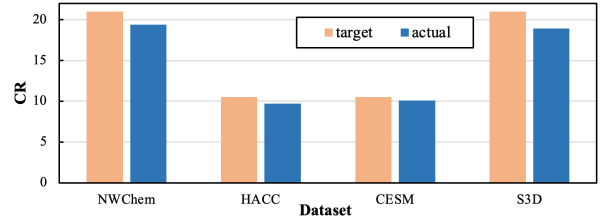


Figure 13: Comparison of target and actual ratio in fixed-ratio mode.

4.7 Evaluation on Fixed-Ratio Mode

As discussed in Section 3, our novel compression engine has two working modes: fixed-accuracy mode (i.e. error-bounded mode) and fixed-ratio mode (i.e., fixed bit-rate mode). The fixed-ratio mode can allow the system have a consistent throughput for data transfer. To verify the effectiveness of our fixed-ratio mode, we set the target compression ratios of 10.5 and 21 for single and double floating-point data, respectively. Figure 13 shows the compression between the target compression ratio and the actual compression ratio. The difference is within 15%, which is acceptable in our use case.

4.8 Evaluation on Ratio and Distortion

Compression ratio is defined as the ratio of original data size to the compressed data size. PSNR is a widely used indicator to assess the distortion of data after lossy compression, which is calculated as:

$$\text{PSNR} = 20 \cdot \log_{10} \left[(d_{\max} - d_{\min}) / \text{RMSE} \right]. \quad (3)$$

N is the number of data points and d_{\max} and d_{\min} are the maximal and minimal values, respectively. RMSE is the *root mean squared error*, i.e., $\sqrt{\frac{1}{N} \sum_{i=1}^N (d_i - d_i^*)^2}$, where d_i and d_i^* are the original and decompressed data values, respectively. The larger the PSNR, the lower the RMSE, meaning lower distortion of reconstructed data and hence more accurate post analysis.

Figure 14 shows the comparison of compression ratio among BurstZ, CEAZ, and CPU-SZ on our test datasets with different value-range-based relative error bounds of $1e-3 \sim 1e-6$. The compression ratio of our CEAZ is notably higher than that of BurstZ. CEAZ consistently provides $3 \times \sim 10 \times$ higher compression ratio than BurstZ under the same error bound. Particularly, our CEAZ improves the compression ratio by up to $12 \times$ on the Brown dataset over BurstZ when the error bound is equal to $1e-3$. Compared to the CPU-SZ, the degradation of compression ratio is within 10% on all test datasets and error bounds. This result demonstrates the effectiveness of our adaptive strategy and offline codewords.

We also compare the compression ratio and throughput among LZ4, Gzip, and CEAZ, as shown in Table 4. We use the best compression mode for LZ4 and Gzip. The table illustrates that CEAZ is effective to reduce the scientific data size with high throughput.

Table 4: Comparison of compression ratio and averaged throughput (in GB/s) among LZ4, Gzip, CEAZ, and CPU-SZ on test datasets.

	eb	NWChem	Brown	CESM	S3D	throughput
LZ4	N/A	1.01	1.06	1.18	1.05	1.5
Gzip	N/A	1.05	1.24	1.51	1.14	1.3
CEAZ	$1e-4$	28.2	46.2	9.1	30.9	16.5
CPU-SZ	$1e-4$	30.6	49.3	13.1	41.3	0.2

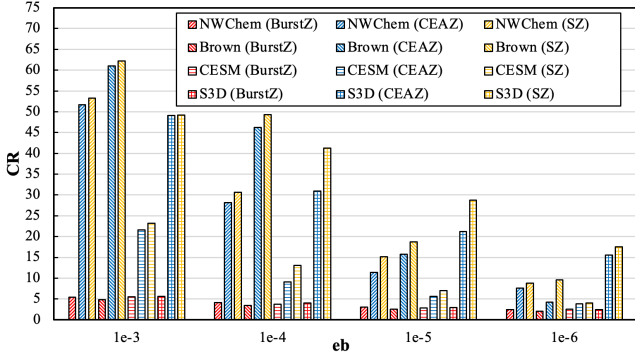


Figure 14: Compression ratio comparison among BurstZ, CEAZ, SZ.

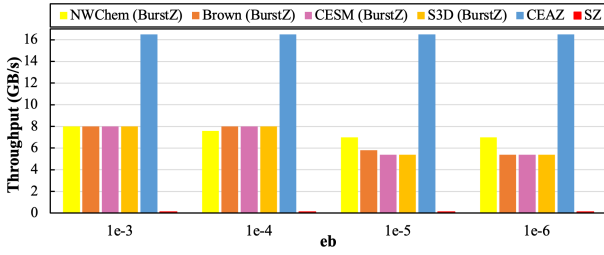


Figure 15: Throughput comparison among BurstZ, CEAZ, CPU-SZ.

In addition, Table 5 shows the comparison of distortion (PSNR) between CEAZ and CPU-SZ under different error bounds. The degradation of PSNR is within 3 dB under very high PSNRs (all higher than 60 dB).

Table 5: Distortion (i.e., PSNR) comparison between CEAZ and SZ under different error bounds.

eb	NWChem		Brown		CESM		S3D	
	SZ	CEAZ	SZ	CEAZ	SZ	CEAZ	SZ	CEAZ
1e-3	67.5	70.1	64.7	64.8	64.8	63.7	69.2	65.9
1e-4	86.7	90.4	84.7	83.8	85.9	84.3	85.4	87.1
1e-5	105.1	107.7	104.8	104.6	105.3	103.6	104.7	108.6
1e-6	124.9	126.0	124.8	124.5	125.4	124.7	124.9	128.6

4.9 Evaluation on Time, Latency & Throughput

The time of the entire compression process (excluding the file loading and dumping time) is measured as the period from the moment that FPGA receives the data through the moment that the whole compression is finished with output bytes. We show the comparison of compression time among BurstZ, CEAZ, and CPU-SZ in Table 6. “ebs” represents all error bounds from 1e-3 to 1e-6. We observe that CEAZ reduces the time by up to 67% compared with the second-best BurstZ on the same dataset.

Moreover, we evaluate the latency of CPU-SZ, cuSZ (GPU), cuZFP (GPU), and CEAZ (FPGA) on small datasets (i.e., $16^2 \sim 128^2$), as shown in Table 7. The test small data are chunked from CESM-ATM datasets. The table illustrates that CEAZ achieves up to 587.8× and 25.6× lower latency than cuSZ and cuZFP, respectively.

Table 6: Compression time (in second) of different compressors.

	eb	NWChem	Brown	CESM	S3D
BurstZ	1e-3	2.0	3.1e-2	1.8e-1	5.5
BurstZ	1e-4	2.1	3.1e-2	1.8e-1	5.5
BurstZ	1e-5	2.3	4.3e-2	2.7e-1	8.1
BurstZ	1e-6	2.3	4.6e-2	2.7e-1	8.1
CEAZ	ebs	1.0	1.5e-2	8.9e-2	2.7
CPU-SZ	ebs	131.1	2.0	12.0	360.7

Table 7: Latency (μ s) of different lossy compressors on small data.

	CPU-SZ	cuSZ (GPU)	cuZFP (GPU)	CEZA (FPGA)
1 KB	119	423.2	17.9	0.7
4 KB	150	507.6	19.7	1.7
16 KB	466	563.5	27.2	5.5
64 KB	5699	631.7	46.1	20.9

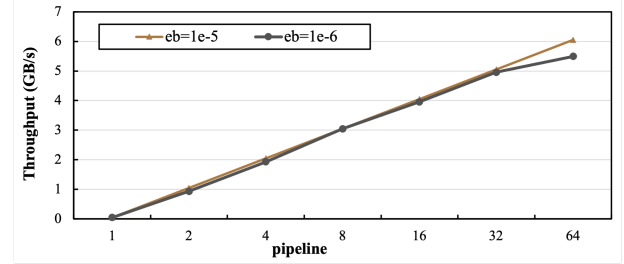


Figure 16: Compression throughputs with multiple pipelines.

Throughput is defined as the number of data points processed (such as compression) per second. Figure 15 shows the comparison of throughput among BurstZ, CEAZ, and CPU-SZ across four datasets and four error bounds. CEAZ can consistently provide about 16 GB/s throughput with different error bound settings, which is 2× higher than BurstZ.

It is worth noting that CEAZ can provide at least 4× higher compression ratio compared to BurstZ. Due to such a high compression ratio (or high data reduction capability), the bandwidth of dumping compressed data (even with the smallest compression ratio) is still less than the bandwidth capacity of the Ethernet transceiver in our FPGA board (i.e., 100 Gb/s), thereby, the overall throughput has not been bounded by this capacity. Moreover, our clock frequency is around 265 MHz, thus the throughput could be further improved by increasing the frequency. In addition, compared with the serial CPU-SZ, CEAZ improves the overall throughput by up to 135×.

4.10 Parallel Performance Evaluation

We demonstrate the parallel performance in two ways. First, we evaluate the throughput of CEAZ with different parallel pipelines in the single FPGA board. Second, we evaluate CEAZ with multiple nodes for parallel performance improvement.

4.10.1 Multi-pipeline Evaluation. We choose CESM-ATM as a test dataset and set the value-range-based error bound to 1e-5 or 1e-6, which is commonly used in the CESM application [37]. We increase the compression pipelines from 1 to 64. Figure 16 illustrates that the throughput increases linearly as the number of pipelines increases (except 64 pipelines with the error bound of 1e-6). CEAZ can achieve this high scalability because (1) our compression engine reads data

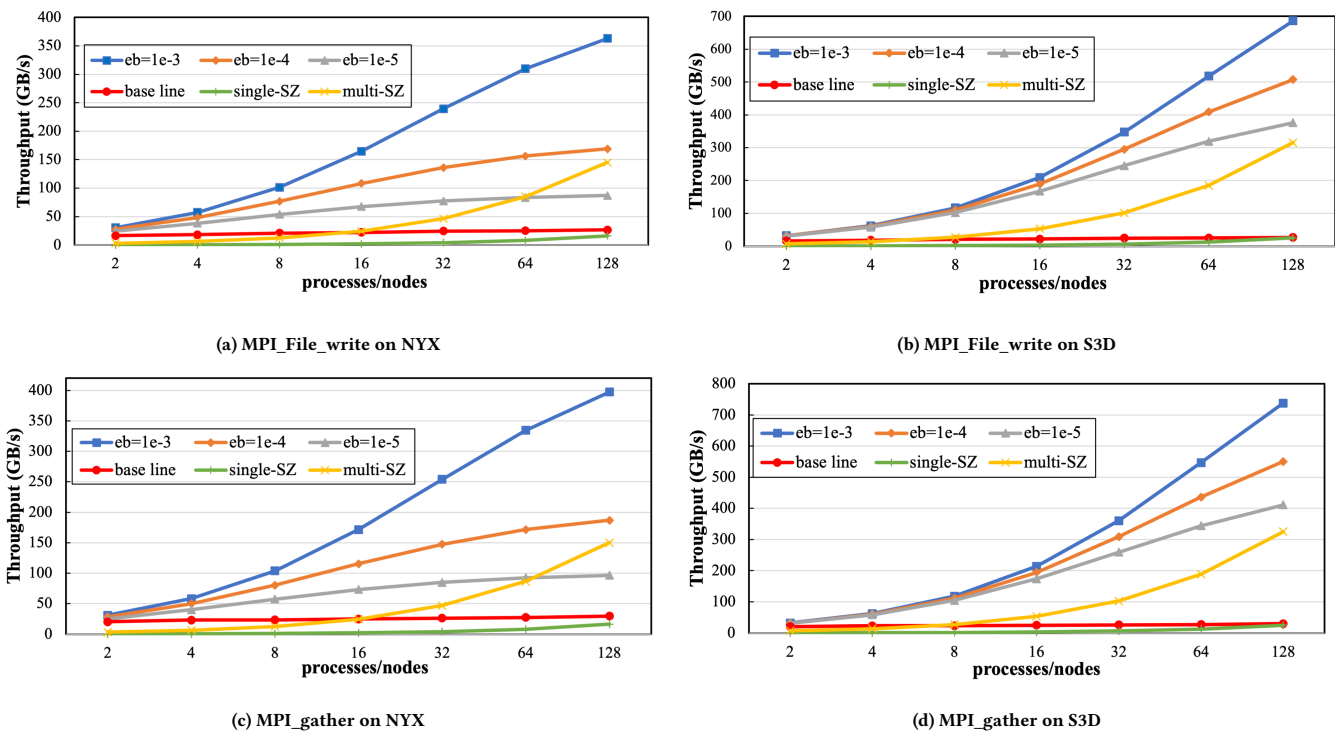


Figure 17: Throughput comparison of CEAZ-accelerated and original MPI operations (i.e., MPI_File_write and MPI_Gather) on NYX and S3D with different numbers of processes/nodes. “single-SZ” denotes SZ with a single CPU core/node. “multi-SZ” denotes SZ with 16 CPU cores/node.

from HMB2 with a very high bandwidth of 460 GB/s, and (2) our compression engine adopts dual-quant to fully remove the data dependency so that we can process different chunks of the dataset in parallel. The reason for the degradation from 32 pipelines to 64 pipelines with the error bound of $1e-6$ is that the bandwidth of dumping compressed data reaches the bandwidth capacity of the Ethernet transceiver (i.e., 100 Gb/s). Note that this degradation does not happen to the error bound of $1e-5$ because $1e-5$ has higher compression ratio (i.e., smaller compressed size) than $1e-6$, hence later reaching the transceiver bandwidth capacity.

4.10.2 Multi-node Evaluation. We evaluate the performance improvements of MPI collective and MPI-IO operations gained from CEAZ. Specifically, we evaluate the MPI_File_write and MPI_Gather. We conduct our experiments with up to 128 nodes (one process per node). Each node holds a copy of datasets for compression and transmission, i.e., 3.0 GB of NYX and 10.2 GB of S3D per node. Thus, the overall data size for parallel I/O is up to 1.3 TB with 128 nodes. We evaluate CPU-SZ on both a single core and 16 cores with the error bound of $1e-3$. Table 8 shows the compression ratio of CPU-SZ and CEAZ on NYX and S3D with different error bounds.

Table 8: Compression ratio of CPU-SZ and CEAZ on NYX and S3D.

	NYX		S3D	
	CPU-SZ	CEAZ	CPU-SZ	CEAZ
1e-3	23.1	20.3	49.2	47.3
1e-4	10.4	8.5	41.3	30.9
1e-5	5.5	4.2	28.8	21.1

Figure 17a and Figure 17b show the MPI-IO throughputs on the NYX and S3D datasets with different approaches. The throughput of original MPI_File_write (without compression) increases slightly as the number of nodes increases and reaches 26.6 GB/s with 128 nodes in Bridges-2, as shown as the baselines in the figures. The single-core-SZ-supported MPI_File_write only achieves an overall throughput of up to 23.9 GB/s (including CPU-SZ compression time and time to write compressed data in parallel) when using 128 nodes, which is still 10.2% lower than the baseline. This is because the compression throughput of CPU-SZ (i.e., about 204.8 MB/s per node) is not fast enough compared to the state-of-the-art interconnect such as InfiniBand HDR with a bandwidth of 200Gb/s. The multi-core-SZ-supported MPI_File_write can provide an overall throughput of up to 315.1 GB/s when using 128 nodes, which is 11.8× higher than the baseline. In comparison, CEAZ-supported MPI_File_write can improve the overall throughput (including CEAZ compression time and time to write compressed data in parallel) by up to 13.6 and 25.8 on NYX and S3D, respectively.

Figure 17c and Figure 17d show the MPI_Gather throughputs on the NYX and S3D datasets with different approaches. The throughput of original MPI_Gather reaches 29.7 GB/s with 128 nodes in Bridges-2, as shown as the baselines in the figures. Similar to MPI_File_write, the single-core-SZ-supported MPI_Gather only achieves an overall throughput of up to 25.1 GB/s with 128 nodes, which is still 15.5% lower than the baseline, whereas the multi-core-SZ-supported MPI_Gather can provide an overall throughput of up to 325.1 GB/s when using 128 nodes, which is 10.9× higher than the

baseline. In comparison, CEAZ-supported MPI_Gather can improve the overall throughput by up to 13.4× and 24.8×, respectively.

5 CONCLUSION

In this work, we propose a hardware-algorithm co-design of efficient and adaptive lossy compressor for scientific data (called CEAZ). To achieve both high compression ratio and throughput, we propose an efficient Huffman coding approach that can adaptively update Huffman codewords online based on our offline generated representative Huffman codewords. We also derive a theoretical analysis to accurately control compression ratio under the error-bounded compression mode, enabling an accurate generation of offline Huffman codewords and a fixed-ratio compression mode. Our evaluation demonstrates that CEAZ outperforms the second-best FPGA-based error-bounded lossy compressor by 2× of throughput and 9.6× of compression ratio. CEAZ can also improve MPI_File_write and MPI_Gather by up to 25.8× and 24.8×, respectively, with 128 nodes in Bridges-2 supercomputer.

REFERENCES

- [1] Ann S Almgren, John B Bell, Mike J Lijewski, Zarija Lukić, and Ethan Van Andel. 2013. Nyx: A massively parallel amr code for computational cosmology. *The Astrophysical Journal* 765, 1 (2013), 39.
- [2] Ian Blanes, Miguel Hernández-Cabronero, Joan Serra-Sagrastà, and Michael W Marcellin. 2019. Lower bounds on the redundancy of Huffman codes with known and unknown probabilities. *IEEE Access* 7 (2019), 115857–115870.
- [3] Bridges-2. 2021. <https://www.psc.edu/resources/bridges-2/>. Online.
- [4] Bridges-2 Data Infrastructure. 2021. https://www.xsede.org/documents/10165/2374841/Bridges-2+Intro_ECSS_Symposium_102020.pdf/4adfe227-6950-41d5-9988-e526eaf8eba9. Online.
- [5] Brown-Samples by Brown University. 2019. <https://sdrbench.github.io/>. Online.
- [6] Martin Burtcher and Paruj Ratanaworabhan. 2008. FPC: A high-speed compressor for double-precision floating-point data. *IEEE Trans. Comput.* 58, 1 (2008), 18–31.
- [7] Franck Cappello, Sheng Di, Sihuan Li, Xin Liang, Ali Murat Gok, Dingwen Tao, Chun Hong Yoon, Xin-Chuan Wu, Yuri Alexeev, and Frederic T Chong. 2019. Use cases of lossy compression for floating-point data in scientific data sets. *The International Journal of High Performance Computing Applications* (2019).
- [8] Community Earth System Model (CESM) Atmosphere Model. 2019. <http://www.cesm.ucar.edu/models/>. Online.
- [9] cuZFP. 2021. https://github.com/LLNL/zfp/tree/develop/src/cuda_zfp.
- [10] Sheng Di and Franck Cappello. 2016. Fast error-bounded lossy HPC data compression with SZ. In 2016 IEEE International Parallel and Distributed Processing Symposium. IEEE, 730–739.
- [11] Sheng Di and Franck Cappello. 2016. Fast error-bounded lossy HPC data compression with SZ. In 2016 IEEE International Parallel and Distributed Processing Symposium. IEEE, IEEE, Chicago, IL, USA, 730–739.
- [12] Daniel Firestone, Andrew Putnam, Sambhrama Mundkur, Derek Chiou, Alireza Dabagh, Mike Andrewartha, Hari Angepat, Vivek Bhanu, Adrian Caulfield, Eric Chung, et al. 2018. Azure accelerated networking: Smartnics in the public cloud. In 15th {USENIX} Symposium on Networked Systems Design and Implementation ({NSDI} 18). 51–66.
- [13] Mike Folk, Gerd Heber, Quincey Koziol, Elena Pourmal, and Dana Robinson. 2011. An overview of the HDF5 technology suite and its applications. In Proceedings of the EDBT/ICDT 2011 Workshop on Array Databases. 36–47.
- [14] Brian Friesen, Ann Almgren, Zarija Lukić, Gunther Weber, Dmitriy Morozov, Vincent Beckner, and Marcus Day. 2016. In situ and in-transit analysis of cosmological simulations. *Computational Astrophysics and Cosmology* 3, 1 (2016), 1–18.
- [15] Tong Geng, Tianqi Wang, Chunshu Wu, Chen Yang, Wei Wu, Ang Li, and Martin C. Herbordt. 2019. O3BNN: an out-of-order architecture for high-performance binarized neural network inference with fine-grained pruning. In Proceedings of the ACM International Conference on Supercomputing. ACM, Denver, CO, USA, 461–472.
- [16] Ali Murat Gok, Sheng Di, Yuri Alexeev, Dingwen Tao, Vladimir Mironov, Xin Liang, and Franck Cappello. 2018. Pastr: Error-bounded lossy compression for two-electron integrals in quantum chemistry. In 2018 IEEE international conference on cluster computing (CLUSTER). IEEE, 1–11.
- [17] William Gropp, Ewing Lusk, Nathan Doss, and Anthony Skjellum. 1996. A high-performance, portable implementation of the MPI message passing interface standard. *Parallel computing* 22, 6 (1996), 789–828.
- [18] Pascal Grosset, Christopher Biber, Jesus Pulido, Arvind Mohan, Ayan Biswas, John Patchett, Terece Turton, David Rogers, Daniel Livescu, and James Ahrens. 2020. Foresight: analysis that matters for data reduction. In 2020 SC20: International Conference for High Performance Computing, Networking, Storage and Analysis (SC). IEEE Computer Society, 1171–1185.
- [19] HACC team (ECP EXASKY). 2019. <https://sdrbench.github.io/>. Online.
- [20] Pouya Haghi, Anqi Guo, Qingqing Xiong, Rushi Patel, Chen Yang, Tong Geng, Justin T Broadus, Ryan Marshall, Anthony Skjellum, and Martin C Herbordt. 2020. FPGAs in the Network and Novel Communicator Support Accelerate MPI Collectives. In 2020 IEEE High Performance Extreme Computing Conference (HPEC). IEEE, 1–10.
- [21] Katrin Heitmann, Thomas D Uram, Hal Finkel, Nicholas Frontiere, Salman Habib, Adrian Pope, Esteban Rangel, Joseph Hollowed, Danila Korytov, Patricia Larsen, Benjamin S. Allen, Kyle Chard, and Ian Foster. 2019. HACC Cosmological Simulations: First Data Release. *arXiv preprint arXiv:1904.11966* (2019).
- [22] D. A. Huffman. 1952. A Method for the Construction of Minimum-Redundancy Codes. *Proceedings of the IRE* 40, 9 (Sep. 1952), 1098–1101.
- [23] Lawrence Ibarria, Peter Lindstrom, Jarek Rossignac, and Andrzej Szymczak. 2003. Out-of-core compression and decompression of large n-dimensional scalar fields. In *Computer Graphics Forum*, Vol. 22. Wiley Online Library, 343–348.
- [24] Sian Jin, Pascal Grosset, Christopher M Biber, Jesus Pulido, Jiannan Tian, Dingwen Tao, and James Ahrens. 2020. Understanding GPU-Based Lossy Compression for Extreme-Scale Cosmological Simulations. *arXiv preprint arXiv:2004.00224* (2020).
- [25] Sian Jin, Jesus Pulido, Pascal Grosset, Jiannan Tian, Dingwen Tao, and James Ahrens. 2021. Adaptive Configuration of In Situ Lossy Compression for Cosmology Simulations via Fine-Grained Rate-Quality Modeling. *arXiv preprint arXiv:2104.00178* (2021).
- [26] Ryan Kastner, Janarbek Matai, and Stephen Neuendorffer. 2018. Parallel programming for FPGAs. *arXiv preprint arXiv:1805.03648* (2018).
- [27] Hemanth Kolla. 2019. <https://sdrbench.github.io/>. Online.
- [28] Sohan Lal, Jan Lucas, and Ben Juurlink. 2017. E² 2MC: Entropy Encoding Based Memory Compression for GPUs. In 2017 IEEE International Parallel and Distributed Processing Symposium (IPDPS). IEEE, 1119–1128.
- [29] Xin Liang, Sheng Di, Dingwen Tao, Sihuan Li, Shaomeng Li, Hanqi Guo, Zizhong Chen, and Franck Cappello. 2018. Error-Controlled Lossy Compression Optimized for High Compression Ratios of Scientific Datasets. (2018).
- [30] Peter Lindstrom. 2014. Fixed-rate compressed floating-point arrays. *IEEE Transactions on Visualization and Computer Graphics* 20, 12 (2014), 2674–2683.
- [31] Peter Lindstrom and Martin Isenburt. 2006. Fast and efficient compression of floating-point data. *IEEE Transactions on Visualization and Computer Graphics* 12, 5 (2006), 1245–1250.
- [32] Jay F Lofstead, Scott Klasky, Karsten Schwan, Norbert Podhorszki, and Chen Jin. 2008. Flexible IO and integration for scientific codes through the adaptable IO system (ADIOS). In Proceedings of the 6th international workshop on Challenges of large applications in distributed environments. 15–24.
- [33] Tao Lu, Qing Liu, Xubin He, Huizhang Luo, Eric Suchyta, Jong Choi, Norbert Podhorszki, Scott Klasky, Mathew Wolf, Tong Liu, et al. 2018. Understanding and modeling lossy compression schemes on HPC scientific data. In 2018 IEEE International Parallel and Distributed Processing Symposium. IEEE, 348–357.
- [34] Huizhang Luo, Dan Huang, Qing Liu, Zhenbo Qiao, Hong Jiang, Jing Bi, Haitao Yuan, Mengchu Zhou, Jinzhen Wang, and Zhenlu Qin. 2019. Identifying Latent Reduced Models to Precondition Lossy Compression. In 2019 IEEE International Parallel and Distributed Processing Symposium. IEEE.
- [35] Masahiro Nakao, Koji Ueno, Katsuki Fujisawa, Yuetsu Kodama, and Mitsuhsa Sato. 2020. Performance Evaluation of Supercomputer Fugaku using Breadth-First Search Benchmark in Graph500. In 2020 IEEE International Conference on Cluster Computing (CLUSTER). IEEE, 408–409.
- [36] NWChem - Open Source High-Performance Computational Chemistry. 2019. <https://nwchemgit.github.io/>. Online.
- [37] Andrew Poppick, Joseph Nardi, Noah Feldman, Allison H Baker, Alexander Pinard, and Dorit M Hammerling. 2020. A statistical analysis of lossily compressed climate model data. *Computers & Geosciences* 145 (2020), 104599.
- [38] Andrew Putnam, Adrian M Caulfield, Eric S Chung, Derek Chiou, Kypros Constantinides, John Demme, Hadi Esmaeilzadeh, Jeremy Fowers, Gopi Prashanth Gopal, Jan Gray, et al. 2014. A reconfigurable fabric for accelerating large-scale data-center services. In 2014 ACM/IEEE 41st International Symposium on Computer Architecture (ISCA). IEEE, 13–24.
- [39] Scientific Data Reduction Benchmarks. 2019. <https://sdrbench.github.io/>. Online.
- [40] Seung Woo Son, Zhengzhang Chen, William Hendrix, Ankit Agrawal, Wei-keng Liao, and Alok Choudhary. 2014. Data compression for the exascale computing era-survey. *Supercomputing Frontiers and Innovations* 1, 2 (2014), 76–88.
- [41] Gongjin Sun, Seoungyoung Kang, and Sang-Woo Jun. 2020. BurstZ: a bandwidth-efficient scientific computing accelerator platform for large-scale data. In Proceedings of the 34th ACM International Conference on Supercomputing. 1–12.

- [42] System Management Interface. 2021. <https://developer.nvidia.com/nvidia-system-management-interface>. Online.
- [43] Dingwen Tao, Sheng Di, Zizhong Chen, and Franck Cappello. 2017. In-depth exploration of single-snapshot lossy compression techniques for N-body simulations. In *2017 IEEE International Conference on Big Data*. IEEE, 486–493.
- [44] Dingwen Tao, Sheng Di, Zizhong Chen, and Franck Cappello. 2017. Significantly improving lossy compression for scientific data sets based on multidimensional prediction and error-controlled quantization. In *2017 IEEE International Parallel and Distributed Processing Symposium*. IEEE, 1129–1139.
- [45] Dingwen Tao, Sheng Di, Xin Liang, Zizhong Chen, and Franck Cappello. 2019. Optimizing Lossy Compression Rate-Distortion from Automatic Online Selection between SZ and ZFP. *IEEE Transactions on Parallel and Distributed Systems* (2019).
- [46] David Taubman and Michael Marcellin. 2012. *JPEG2000 image compression fundamentals, standards and practice: image compression fundamentals, standards and practice*. Vol. 642. Springer Science & Business Media.
- [47] Jiannan Tian, Sheng Di, Chengming Zhang, Xin Liang, Sian Jin, Dazhao Cheng, Dingwen Tao, and Franck Cappello. 2020. Wavesz: A hardware-algorithm co-design of efficient lossy compression for scientific data. In *Proceedings of the 25th ACM SIGPLAN Symposium on Principles and Practice of Parallel Programming*. 74–88.
- [48] Jiannan Tian, Sheng Di, Kai Zhao, Cody Rivera, Megan Hickman Fulp, Robert Underwood, Sian Jin, Xin Liang, Jon Calhoun, Dingwen Tao, and Franck Cappello. 2020. cuSZ: An Efficient GPU-Based Error-Bounded Lossy Compression Framework for Scientific Data. (2020), 3–15.
- [49] Jiannan Tian, Cody Rivera, Sheng Di, Jieyang Chen, Xin Liang, Dingwen Tao, and Franck Cappello. 2021. Revisiting Huffman Coding: Toward Extreme Performance on Modern GPU Architectures. In *2021 IEEE International Parallel and Distributed Processing Symposium (IPDPS)*, Portland, OR, USA, May 17-21, 2021. IEEE, 881–891.
- [50] Vitis Libraries. 2020. https://github.com/Xilinx/Vitis_Libraries/. Online.
- [51] Vitis Unified Software Platform. 2020. <https://www.xilinx.com/products/design-tools/vitis/vitis-platform.html>. Online.
- [52] Lipeng Wan, Matthew Wolf, Feiyi Wang, Jong Youl Choi, George Ostrouchov, and Scott Klasky. 2017. Analysis and modeling of the end-to-end i/o performance on olcf’s titan supercomputer. In *2017 IEEE 19th International Conference on High Performance Computing and Communications; IEEE 15th International Conference on Smart City; IEEE 3rd International Conference on Data Science and Systems (HPCC/SmartCity/DSS)*. IEEE, 1–9.
- [53] Lipeng Wan, Matthew Wolf, Feiyi Wang, Jong Youl Choi, George Ostrouchov, and Scott Klasky. 2017. Comprehensive measurement and analysis of the user-perceived I/O performance in a production leadership-class storage system. In *2017 IEEE 37th International Conference on Distributed Computing Systems (ICDCS)*. IEEE, 1022–1031.
- [54] Xin-Chuan Wu, Sheng Di, Emma Maitreyee Dasgupta, Franck Cappello, Hal Finkel, Yuri Alexeev, and Frederic T Chong. 2019. Full-state quantum circuit simulation by using data compression. In *Proceedings of the International Conference for High Performance Computing, Networking, Storage and Analysis*. 1–24.
- [55] Xilinx Power Estimator. 2021. <https://www.xilinx.com/products/technology/power/xpe.html>. Online.
- [56] Qingqing Xiong, Rushi Patel, Chen Yang, Tong Geng, Anthony Skjellum, and Martin C Herbordt. 2019. Ghostsz: A transparent fpga-accelerated lossy compression framework. In *2019 IEEE 27th Annual International Symposium on Field-Programmable Custom Computing Machines (FCCM)*. IEEE, 258–266.
- [57] ZHW - ZFP Hardware Implementation. 2021. <https://github.com/LLNL/zhw/>. Online.